

Evolution of Star Clusters near the Galactic Center: Fully Self-consistent N -body Simulations

M. Fujii^{1,3}, M. Iwasawa^{2,3}, Y. Funato², and J. Makino³

ABSTRACT

We have performed fully self-consistent N -body simulations of star clusters near the Galactic center (GC). Such simulations have not been performed because it is difficult to perform fast and accurate simulations of such systems using conventional methods. We used the Bridge code, which integrates the parent galaxy using the tree algorithm and the star cluster using the fourth-order Hermite scheme with individual timestep. The interaction between the parent galaxy and the star cluster is calculate with the tree algorithm. Therefore, the Bridge code can handle both the orbital and internal evolutions of star clusters correctly at the same time. We investigated the evolution of star clusters using the Bridge code and compared the results with previous studies. We found that 1) the inspiral timescale of the star clusters is shorter than that obtained with "traditional" simulations, in which the orbital evolution of star clusters is calculated analytically using the dynamical friction formula and 2) the core collapse of the star cluster increases the core density and help the cluster survive. The initial conditions of star clusters is not so severe as previously suggested.

Subject headings: galaxy: star clusters — Galaxy: center, kinematics and dynamics — methods: numerical — stellar dynamics

1. Introduction

A few dozens of very young and massive stars have been found in the central parsec of the Galaxy (Krabbe et al. 1995; Paumard et al. 2001, 2006). These stars are a few million years old (Paumard et al. 2001; Ghez 2003) and lie on a disk (Lu et al. 2006) or two disks (Paumard et al. 2006). The disks rotate around the central black hole (BH) and are at large angles with each other. One disk rotates clockwise in projection, the other counterclockwise (Paumard et al. 2006). These disks are coeval to within 1 Myr. The orbit of

the stars on the clockwise rotating disk are circular (Paumard et al. 2006) or eccentric have lower-limit eccentricities of 0.0 – 0.8 (Lu et al. 2006), while those on the counterclockwise disk have high eccentricities at around 0.8 (Paumard et al. 2006). In the central parsec, in situ formation of these stars seems difficult because of the strong tidal field of the central BH. To overcome this difficulty, two possibilities have been suggested: (1) in situ star formation in a massive accretion disk, or (2) inspiraling young star clusters.

The accretion disk scenario was proposed by Levin & Beloborodov (2003). A dense gaseous disk is formed from a molecular cloud which somehow fell to the neighborhood of the central BH. If the disk is sufficiently massive it can become gravitationally unstable, resulting in fragmentation and formation of stars. However, this scenario is problematic. Observations have shown that two disks are at large angles with respect to each other and these stars on the disks formed almost at the same time. In this scenario, two disks must have ex-

¹Department of Astronomy, Graduate School of Science, The University of Tokyo, 7-3-1 Hongo, Bunkyo, Tokyo 113-0033; fujii@cfca.jp

²Department of General System Studies, College of Arts and Sciences, The University of Tokyo, 3-8-1 Komaba, Meguro, Tokyo 153-8902; iwasawa@margaux.astron.s.u-tokyo.ac.jp, funato@artcompsci.org

³Division of Theoretical Astronomy, National Astronomical Observatory of Japan, 2-21-1 Osawa, Mitaka, Tokyo, 181-8588; makino@cfca.jp

isted simultaneously within 1 Myr. Moreover, it is difficult to make stars with eccentric orbit from accretion disks (Nayakshin et al. 2007).

The star cluster inspiral scenario was proposed by Gerhard (2001). A star cluster was formed at a distance of tens of parsecs from the GC and spiraled into the GC due to the dynamical friction. This scenario is supported by the observational fact that two young dense star clusters, the Arches and Quintuplet clusters are observed at the distances of ~ 30 pc from the GC (Figer 2004). Although this scenario can explain two stellar disks without difficulty, numerical simulations have shown that it would take too long time for the star cluster to inspiral to the central parsec unless it was very massive or its initial position is very near from the GC (Portegies Zwart et al. 2003, hereafter PZ03; Gürkan & Rasio 2005).

In these works (PZ03; Gürkan & Rasio 2005), the orbit of the cluster within its parent galaxy was calculated using the dynamical friction formula (Chandrasekhar 1943). With this approach, the inspiral timescale might have been overestimated. In Fujii et al. (2006), we performed fully self-consistent N -body simulations of a satellite galaxy within its parent galaxy and found that the orbital decay of the satellite is much faster than those calculated analytically from the dynamical friction formula. This difference was caused by particles escaped from the satellite. One mechanism is that the direct gravitational forces from escaped particles worked as effective drag force to the satellite. The second mechanism is that escaped particles remain close to the body of the satellite and enhance the dynamical friction. These effect should also work in the case of star clusters. Therefore, a fully self-consistent N -body simulation is necessary to obtain correct results for the orbital evolution of star clusters.

Kim & Morris (2003; hereafter KM03) performed self-consistent N -body simulations of star clusters near the GC. Their results showed that if the initial central density of a star cluster was initially very high ($\sim 10^8 M_\odot \text{pc}^{-3}$), the cluster can deliver stars to the central parsec of the Galaxy. In these simulations, however, the internal evolution of the star clusters was neglected. The stars in their model of star clusters have an equal mass and a large softening length of 0.025pc. Such star clusters experience neither mass segregation nor

core collapse. However, if the core collapse occurs, the core density of a star cluster increases. The initial high density of the core will not be necessary. Thus, it is also important to solve the internal evolution correctly.

Such a fully self-consistent N -body simulation has been impossible with conventional numerical methods. While star clusters need a very accurate scheme such as the combination of fourth-order Hermite scheme and direct force calculation, galaxies contain too many particles to use the direct force calculation. To solve this problem, we have developed a new tree-direct hybrid scheme, the ‘‘Bridge’’ scheme (Fujii et al. 2007). The Bridge scheme enables us to perform fully self-consistent N -body simulations of star clusters within their parent galaxies in a realistic time (less than 2 days with a single GRAPE-6 board).

We performed fully self-consistent N -body simulations of evolution of star clusters within their parent galaxies using the Bridge scheme. We also performed the ‘‘traditional’’ N -body simulations, in which the orbital decay of the star cluster is calculated using the dynamical friction formula for comparison. We found that the inspiral timescale of the star cluster is shorter than that obtained in previous studies. In addition, if the initial orbit of the star cluster is eccentric, the timescale of inspiral is much shorter than that for a cluster in the circular orbit of the same apocenter distance.

The eccentricities of the stars escaped from the star cluster distribute around the eccentricity of the star cluster. Thus, if a star cluster is initially in an eccentric orbit, it naturally explains the rather high eccentricities of the stars in the observed ‘‘disks’’. Also, because of the mass segregation effect, very massive stars (more than $10M_\odot$) remained in the cluster and were brought very close to GC. Thus, we conclude that the timescale problem with the cluster inspiral scenario was partly because of the wrong treatment of the dynamical friction and partly because the limited assumption of the circular orbit, and it is not difficult to make the central stellar disks from inspiraled star clusters.

We describe the simulation method and initial conditions in section 2. In section 3 we show the results of simulations. Section 4 is for summary and discussions.

2. Numerical Simulation

2.1. Models

We adopted a King model with $W_0 = 3$ for the model of a star cluster. Its core radius, r_c , half-mass radius, r_h , and tidal radius, r_t , are 0.087 pc, 0.13 pc, and 0.47 pc, respectively. It consists of 65536 stars and we assigned each star a mass randomly drawn from a Salpeter (1955) initial mass function between 0.3 and $100 M_\odot$, irrespective of position. The total mass of the star cluster, M_{SC} , is $7.9 \times 10^4 M_\odot$. This model imitates the Arches cluster (Nagata et al. 1995), whose mass and velocity dispersion are $7 \times 10^4 M_\odot$ within 0.23 pc and 22 km s^{-1} , respectively (Figer et al. 2002). The Arches cluster is located at ~ 30 pc from the GC. We, however, placed our cluster much closer to the GC, to compare our result with those of PZ03. In table 1, we summarize the model parameters.

We used two galaxy models as a model of the central region of the Galaxy; one includes the central SMBH (galaxy 1) and the other does not (galaxy 2). For the galaxy model 1, we adopted a King model with non-dimensional central potential of $W_0 = 10$. We scaled the density and velocity dispersion of our model at 5 pc from the GC to the those of the Galaxy. The density at 5 pc is $6.8 \times 10^3 M_\odot \text{pc}^{-3}$ and the one-dimensional velocity dispersion is 64 km s^{-1} in our scales, while the observed density at 5 pc is $\rho(5\text{pc}) = 6.9 \times 10^3 M_\odot \text{pc}^{-3}$ (Genzel et al. 2003) and the observed velocity dispersion is 54 km s^{-1} at ~ 4 pc (Genzel et al. 2000). Figure 1 shows the enclosed masses of our model galaxy and the result of Genzel et al. (2003). In this model, the total mass of the galaxy, M_G , is $8 \times 10^7 M_\odot$, and the core radius, $r_{c,G}$, and the half-mass radius, $r_{h,G}$, are 0.66 pc and 21 pc, respectively. We used 2×10^6 particles to model the Galaxy. The mass of a particle of the galaxy is $40 M_\odot$. Since our galaxy model has the finite core size of 0.66pc, the orbital evolution of the star cluster should be reasonably accurate as far as its distance from the GC is more than 1pc.

The galaxy model 2 is a more realistic model of than model 1. It includes a central super-massive black hole (SMBH). This model is based on King model. We put a SMBH at the center of the galaxy with King model $W_0 = 10$ and integrated it for around two crossing times. The central region of the galaxy evolved and its density profile became

cuspy. This model roughly represents the Galactic center between 0.1 and 5 pc. The enclosed mass is shown in figure 1. The total mass and the particle mass of the galaxy are $2.9 \times 10^7 M_\odot$ and $14 M_\odot$, respectively.

The initial position and velocity of the star cluster are shown in table 2. We calculated two orbits; one is circular (model C) and the other is eccentric (model E) for the galaxy model 1, and two eccentric orbits (model B1, B2) for the galaxy model 2. In Model B1, the star cluster has almost the same eccentricity as the previous simulation without SMBH. In Model B2, the eccentricity of the star cluster is lower than Model B1. The orbital elements for the eccentric case were chosen so that the star cluster would survive at least for several orbits. At first, we tried the eccentric orbit with the same orbital energy as that of the circular case. However, in this case, the disruption of the cluster was too fast, unless the orbit is close to circular. Therefore we made the eccentric orbit significantly wider.

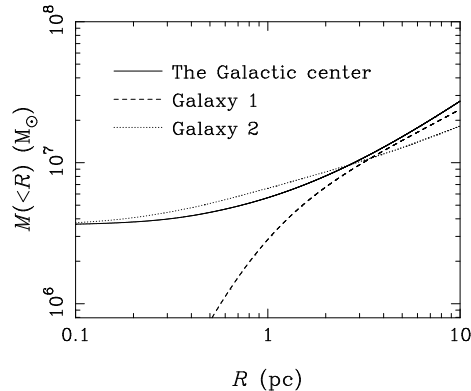


Fig. 1.— Enclosed mass of our model galaxy and the GC (Genzel et al. 2003).

Table 1: Models for the galaxy and the star cluster

	King W_0	N	$M(M_\odot)$	$M_{\text{BH}}(M_\odot)$	r_c (pc)	r_h (pc)	r_t (pc)
Star cluster	3	65536	7.9×10^4	-	0.087	0.13	0.47
Galaxy 1	10	2×10^6	8.0×10^7	-	0.66	21	120
Galaxy 2	10	2×10^6	2.9×10^7	3.6×10^6	-	9.6	72

Table 2: Initial Conditions for the cluster orbit

Simulation	Galaxy model	Orbit	Initial position (pc)	Initial velocity (km/s)
Model C	1	Circular	2	130
Model E	1	Eccentric	5	72
Model B1	2	Eccentric	5	57
Model B2	2	Eccentric	5	67

2.2. Fully Self-consistent N -body Simulation

We performed fully self-consistent N -body simulations using the Bridge code (Fujii et al. 2007). It is a direct-tree hybrid code. Only the internal motion of the star cluster is calculated by the direct scheme with high accuracy, and all other interactions are calculated by the tree algorithm. The splitting between the direct part and tree part is through the splitting of the Hamiltonian in the way similar to MVS (Wisdom & Holman 1991; Kinoshita, Yoshida, & Nakai 1991) or RESPA (Tuckerman et al. 1990). Thus, the low-accuracy calculation of galaxy particles and its interaction with cluster particles are integrated with time-symmetric leapfrog algorithm, resulting in small long-term error. Hence, we can treat a large- N system with embedded small-scale systems fully self-consistently and accurately.

The numerical parameters used for the time integration are summarized in table 3. For the tree part, the Bridge code needs the same parameters with the Barnes-Hut treecode modified for the use with GRAPE hardware (Barnes & Hut 1986; Makino 2004). We used the opening angle $\theta = 0.75$ with the center-of-mass (dipole-accurate) approximation. The maximum group size for a GRAPE calculation (Makino 1991) is 8192. The stepsize of leapfrog integrator is $\Delta t = 1/512$ (in Heggie unit) $= 2.9 \times 10^{-4}$ (Myr) for galaxy 1 and $\Delta t = 1/1024$ (in Heggie unit) $= 1.2 \times 10^{-4}$ (Myr) for galaxy 2. The potential is softened using Plummer softening. The softening length between galaxy particles that between cluster particles and galaxy particles are the same. Both are $\epsilon_G = 3.9 \times 10^{-2}$ pc. For galaxy 2, we adopted the softening length between between the SMBH and galaxy particles, ϵ_{G-BH} , is 0.12 pc and between the SMBH and star cluster particles, ϵ_{SC-BH} , is 0.012 pc.

For the direct part, we used the fourth-order Hermite integrator with block timestep, and the timestep criterion is of the standard Aarseth type (Makino & Aarseth 1992) with $\eta = 0.01$. We also used the Plummer softening for the gravitational force between cluster particles, and we did not model physical collisions or binary formation in the calculation reported in this paper. The softening length between star cluster particles, ϵ_{SC} , is

1.0×10^{-5} pc.

We stopped the simulations at $T = 0.75 - 0.8$ (Myr). Since we used the softening and did not model the physical collision and merging of the stars, the structure of the star cluster after the core collapse might not expressed correctly. We ignored the stellar evolution because we treat only very short time (< 1 Myr) in our simulations.

We used GRAPE-6 (Makino et al. 2003) for force calculation. The total energy was conserved better than 5×10^{-5} for the circular orbit 8×10^{-5} for the eccentric orbit throughout the simulations.

Table 3: Parameters for N -body Simulation

Parameters	Value
ϵ_G	3.9×10^{-2} (pc)
ϵ_{SC}	1.0×10^{-5} (pc)
ϵ_{G-BH}	1.2×10^{-1} (pc)
ϵ_{SC-BH}	1.2×10^{-2} (pc)
Δt (for galaxy 1)	2.9×10^{-4} (Myr)
Δt (for galaxy 2)	1.2×10^{-4} (Myr)
θ	0.75
n_{crit}	8192

2.3. N -body Simulation with Artificial Dynamical Friction

To compare our result with those of previous works, for model C and E, we also performed N -body simulations in which the Galaxy is modeled as a fixed potential and the dynamical friction due to the Galaxy is calculated analytically. This treatment is the same as in PZ03, where the acceleration due to the dynamical friction is calculated using Chandrasekhar's dynamical friction formula (Chandrasekhar 1943; Binney and Tremaine 1987; McMillan & Portegies Zwart 2003)

$$\mathbf{a}_{df} = -4\pi \ln \Lambda \chi G^2 \rho_G M_{SC} \frac{\mathbf{v}_{SC}}{v_{SC}^3}. \quad (1)$$

Here M_{SC} and \mathbf{v}_{SC} are the mass and the center-of-mass velocity of the star cluster, ρ_G is the local density of the Galaxy, $\ln \Lambda$ is the Coulomb logarithm, and

$$\chi \equiv \text{erf}(X) - \frac{2X}{\sqrt{\pi}} \exp(-X^2), \quad (2)$$

where $X = v_{\text{SC}}/\sqrt{2}\sigma_{\text{G}}$ and σ_{G} is the local one-dimensional velocity dispersion of the Galaxy, assumed to be isotropic and locally Maxwellian. For M_{SC} , we adopted the bound mass, which is the total mass of the particles bound to the star cluster. We gave all bound stars the acceleration due to the dynamical friction from the above formula. Unbound stars were not affected by the dynamical friction.

In equation (1), the Coulomb logarithm, $\ln \Lambda$, is given by

$$\ln \Lambda = \ln \left(\frac{b_{\text{max}}}{b_{\text{min}}} \right), \quad (3)$$

where b_{max} and b_{min} are the maximum and minimum impact parameters. It is often set as a constant given by

$$\ln \Lambda \sim \ln \left(\frac{R_{\text{SC}}}{\langle r_{\text{SC}} \rangle} \right), \quad (4)$$

where R_{SC} is the distance of the star cluster from the GC, $\langle r_{\text{SC}} \rangle$ is the characteristic radius of the star cluster (roughly the half-mass radius). PZ03 adopted a constant value, $\chi \ln \Lambda = 1$. However, Hashimoto et al. (2003) found a constant Λ overestimates dynamical friction at pericenter and proposed a variable Λ :

$$\ln \Lambda = \ln \left(\frac{R_{\text{SC}}}{1.4\epsilon_{\text{SC}}} \right), \quad (5)$$

where ϵ_{SC} is the size of the star cluster. We performed N -body simulations with artificial dynamical friction in two ways. One is the same as that used PZ03 (constant Λ), and the other is the way proposed by Hashimoto et al. (2003) (variable Λ). We adopted the virial radius of the star cluster for ϵ_{SC} .

3. Simulation Results

3.1. Circular Orbits

The top panel of figure 2 shows the snapshots of the star clusters projected onto the x-y plane. The top and bottom panels show model C (circular orbit) and E (eccentric orbit), respectively. In model C, the star cluster is initially located at 2 pc from the GC. Due to the tidal field of the Galaxy, the star cluster becomes elongated. Particles stripped from the star cluster form tidal arms and make

ring-like structures. Finally they form a disk-like structure.

We investigated the orbital and internal evolutions of the star cluster. Figure 3 shows the distance of the star cluster from the GC obtained by our N -body simulations. The solid curve shows the result of the full N -body simulation. The dashed and dotted curves show the result of the “traditional” simulations in which the dynamical friction is calculated analytically from the formula with constant Λ and variable Λ , respectively. The orbital decay in the full N -body simulation is faster by 30-40% than that in other simulations. On the other hand, the evolution of the bound mass of the star cluster shown in figure 4 is almost the same among the three. This result suggests that previous studies underestimated the inspiral timescale of star clusters. This effect is not very large, but not negligible.

In figure 4, it seems that the mass loss in the very late stage (after more than 80% of the initial total mass is lost) seems to be significantly slower for the case of full N -body simulation than those for other two simulations, even though the cluster is much closer to GC. This difference is probably due to the finite core size of our galaxy model ($r_c = 0.66\text{pc}$) and not the reality. In order to study the evolution after this stage, we need to use a more realistic model of the mass distribution of the central parsec of the galaxy, which includes the central massive black hole. In addition, stellar collision and merger within the star cluster must be modeled. We are currently working on such an extension of the Bridge code.

Figures 5 and 6 show the core radius and the core density of the star cluster. The core collapse occurred at around $T \simeq 0.53$ Myr. The core collapse times are also the same among the three simulations.

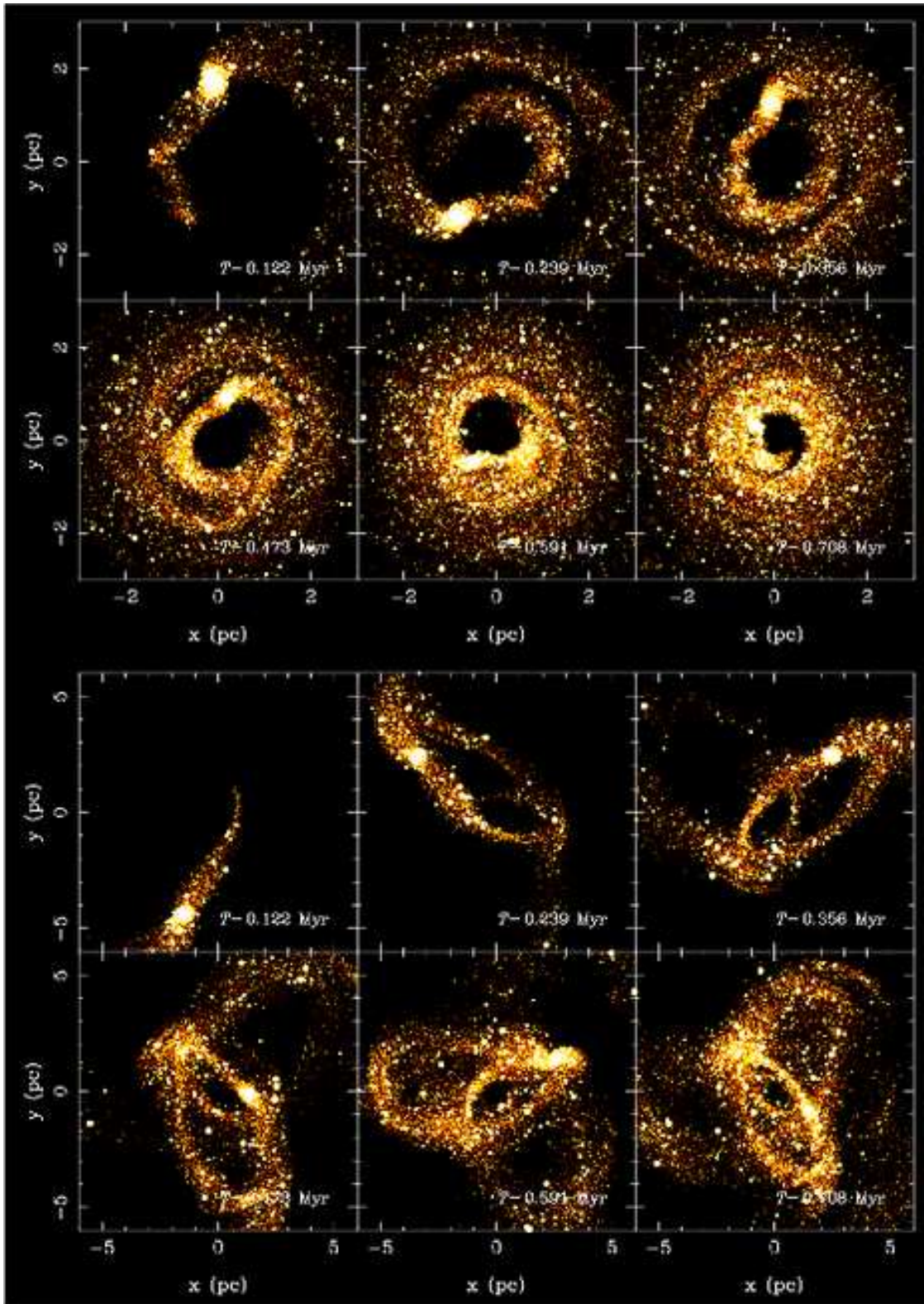


Fig. 2.— Snapshots of the star clusters projected onto $x - y$ plane. The upper six panels are for the run with the circular initial orbit (model C), and the lower six panels are for the run with the eccentric orbit (model E). Times are 0.122, 0.239, 0.356, 0.473, 0.591, and 0.708 Myrs.

3.2. Eccentric Orbits

The bottom panel of figure 2 shows the snapshots of model E projected onto the x-y plane. The initial distance of the star cluster from the GC is 5 pc. The star cluster is elongated and particles are stripped due to the tidal force of the Galaxy. The stripped particles form complex tidal tails.

Figure 7 shows the orbital evolution of the star cluster. The orbital decay of the full N -body simulation is faster than the traditional simulations, as was the case in the runs from the circular orbit. In this case also, the evolution of the bound mass is the same among the three simulations (see figure 8). Moreover, this result shows that variable Λ works better than constant Λ .

Figures 9 and 10 show the core radius and the core density of the star cluster. These show that the core collapse occurred at around $T \simeq 0.55$ Myr. The core collapse time is almost the same as that for the case of the circular orbit, even though the bound mass at the collapse time is different by almost a factor of two. The half-mass relaxation time at the time of the collapse was 0.11 Myr and 0.34 Myr, in model C and E, respectively. Thus, if clusters are rapidly losing its mass due to the tidal field, the apparent age measured by the present relaxation time can show large variations, even if they started from the same initial condition and collapsed at the same time. Furthermore, the core collapse times are the same as that in the case without mass loss due to the tidal field. The core collapse time, t_{cc} , is estimated as $t_{cc} \simeq 0.20t_{rh}$, where t_{rh} is half-mass relaxation time (Portegies Zwart & McMillan 2002). From this equation, we obtain the core collapse time of our model star cluster as 0.51 Myr. Our results agreed with it.

Figure 11 - 14 shows the results of model B1 (dashed curves) and B2 (dotted curves), where the Galaxy model has a central BH. Solid curves show the result of model E (no BH; the same as the solid curve in figure 7 - 10). The orbital evolution of the star cluster in model B1 and B2 is essentially similar to that in model E. However, the orbital decay in model B1 is somewhat slower than that in model E. As is clear in figure 12, in model B1, the mass loss at the pericenter passage is much larger than in the case of model E. Therefore, the core collapse did not occur and the core density

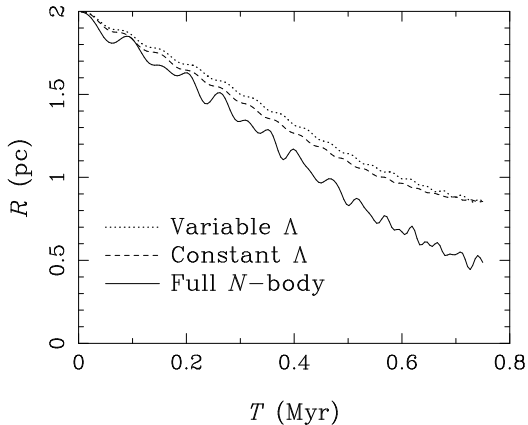


Fig. 3.— The distance of the star cluster from the GC plotted as a function of time for model C. Solid curve shows the result of the full N -body simulation. Dashed and dotted curves show the results of the “traditional” simulations with variable Λ and constant Λ , respectively.

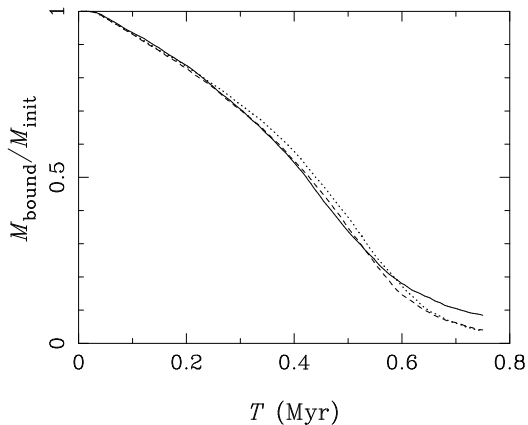


Fig. 4.— The bound mass of the star cluster plotted as a function of time for model C. Curves have the same meanings as in figure 3.

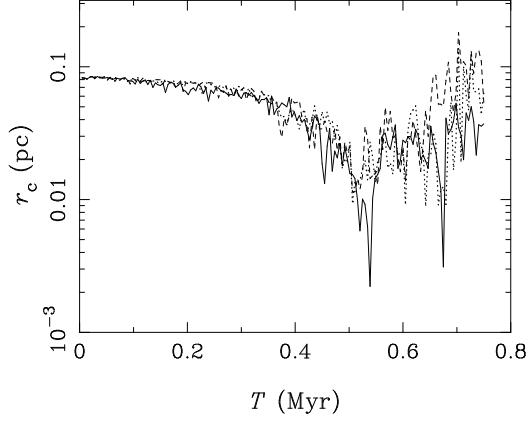


Fig. 5.— The core radius of the star cluster, r_c , plotted as a function of time for model C. Curves have the same meanings as in figure 3.

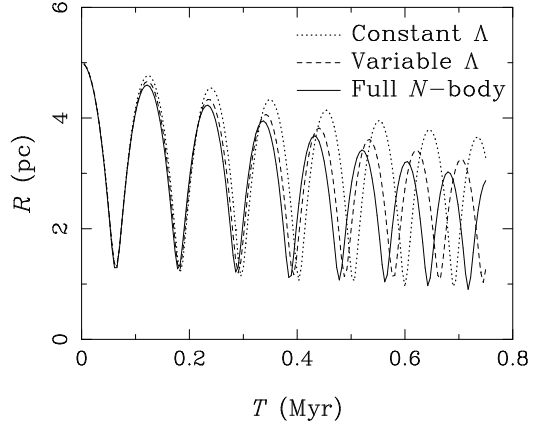


Fig. 7.— The distance of the star cluster from the GC plotted as a function of time for model E. Solid curve shows the result of the full N -body simulation. Curves have the same meanings as in figure 3.

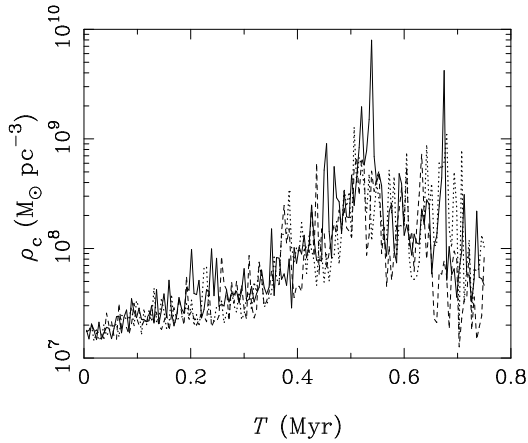


Fig. 6.— The core density of the star cluster, ρ_c , plotted as a function of time for model C. Curves have the same meanings as in figure 3.

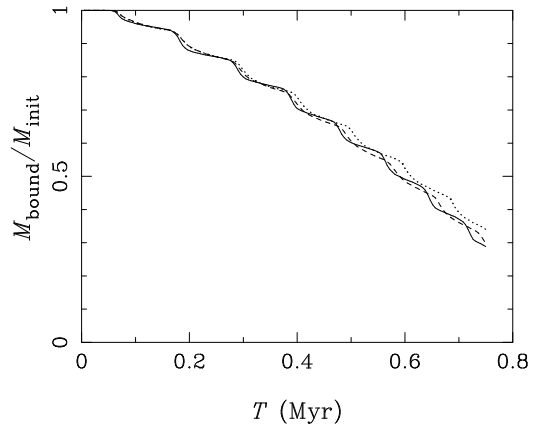


Fig. 8.— The bound mass of the star cluster plotted as a function of time for model E. Curves have the same meanings as in figure 7.

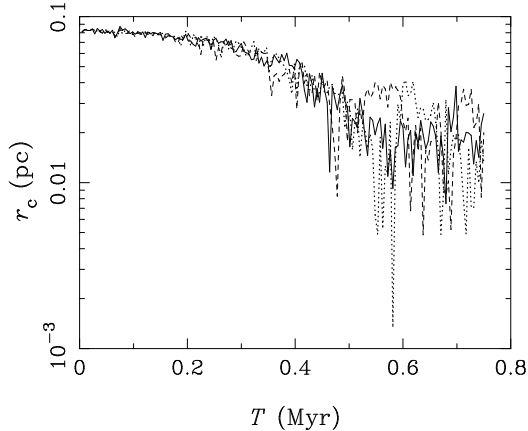


Fig. 9.— The core radius of the star cluster, r_c , plotted as a function of time for model E. Curves have the same meanings as in figure 7.

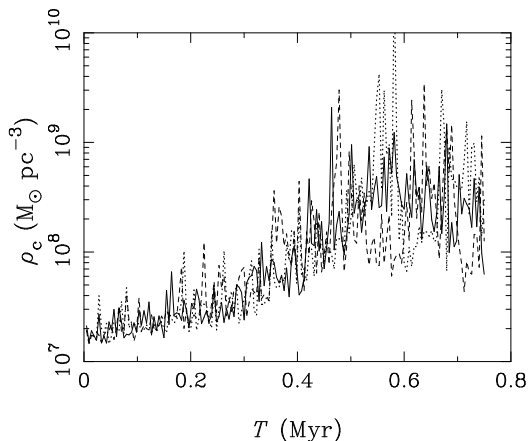


Fig. 10.— The core density of the star cluster, ρ_c , plotted as a function of time for model E. Curves have the same meanings as in figure 7.

of the cluster did not increase. This is because the star cluster suffers the strong tidal force from the SMBH at the pericenter. The small mass of the star cluster slows the orbital evolution of the star cluster. Furthermore, the strong tidal field disrupts the star cluster much faster than the case without SMBH.

In model B2, the pericenter of the star cluster is farther than that in model B1. The evolution of the bound mass is the same as the case without SMBH. However, the orbital evolution is much slower than that of model B1, because the pericenter of the star cluster is farther.

The cluster model and its orbital evolutions in model E and B1 are almost the same as simulation 8 of KM03. Their model of the Galaxy has a power-law density profile with the central SMBH, while our galaxy model 1 for model E has no SMBH. However, the enclosed mass of the galaxy in KM03 is very similar to ours between around 1 and 10 pc. In their simulation, the star cluster was totally disrupted before 1 Myr, but in our simulation, the star cluster has 30% of its initial mass at the end of our simulation (0.75 Myr). The difference is caused by the internal evolution of the star cluster. In our simulation, mass segregation and core collapse of the cluster made the central density much higher, which prevent the complete disruption of the cluster. On the other hand, in KM03, such an evolution was prevented by the numerical method they used.

On the other hand, the cluster in model B1 was disrupted before the core collapse occurs by the strong tidal field of the central SMBH. At around 1 pc, the enclosed mass of galaxy model 2 which includes a SMBH is twice as large as that of K04's model. Such a difference of the enclosed masses is caused by the mass of the SMBH. We adopted $3.6 \times 10^6 M_\odot$ (Eisenhauer et al. 2005), while KM03 did $2.5 \times 10^6 M_\odot$.

Thus, the presence of a SMBH has considerable effect on the evolution of star clusters. The main effect is that the tidal field near the GC becomes much stronger, resulting in faster mass loss from star clusters and preventing its core collapse. In the models we tested, the core collapse time is about the same as the time of the complete disruption in model B1. If the core collapse time is somewhat faster, it is possible that the cluster survives and approaches to the GC. In particular,

if an IMBH is formed within the star cluster, it would significantly help the survival of the cluster. We will study this aspect in more details in the forthcoming papers.

3.3. Eccentricities and Inclinations of the Escaped Stars

For some of the stars in the central parsec, the projected positions and the proper motions have been measured, and their orbital elements have been estimated (Paumard et al. 2006; Lu et al. 2006). Young and bright stars apparently belong to one of the two “disks” (clockwise and counter-clockwise rotating disks), though the existence of the counter-clockwise disk is controversial (Lu et al. 2006). The eccentricities of the stars on the counter-clockwise rotating disk are high, ~ 0.8 (Paumard et al. 2006). For the stars on the clockwise rotating disk, Paumard et al. (2006) concluded their orbits are circular, while Lu et al. (2006) concluded the lower limits of their eccentricities distribute between 0.0 and 0.8. These high eccentricities are difficult to explain with the in-situ formation scenario, and also have been thought to be difficult to explain with cluster in-spiral scenario, since in both cases the stars would have close-to-circular orbits.

We investigated the eccentricities, e , and inclinations, i , of stars escaped from the star cluster (i.e. unbound stars) for model C and E. Figures 15 and 16 show the eccentricities and inclinations of escaped stars and their evolutions for model C and E, respectively. In these figures, the x -axis is the semi-major axis, a , of the star. The eccentricity is defined as $e = (r_a - r_p)/(r_a + r_p)$, where r_a and r_p are the apocenter and pericenter distances, respectively. We obtained the pericenter and apocenter distances by integrating the orbits of the stars in the model potential. The inclination is defined as $i = \cos^{-1}(h_z/h)$, where h and h_z are the angular momentum and its z component, respectively. The top panels show the eccentricities and inclinations of the stars escaped before $T = 0.15$ Myr. The central gap corresponds to the semi-major axis of the star cluster, and the left and right wings are the stars on the leading and trailing arms, respectively. The distributions of the escaped stars on the $a - e$ and $a - i$ plains expand because of the time-varying gravitational force from the star cluster (see the middle panels).

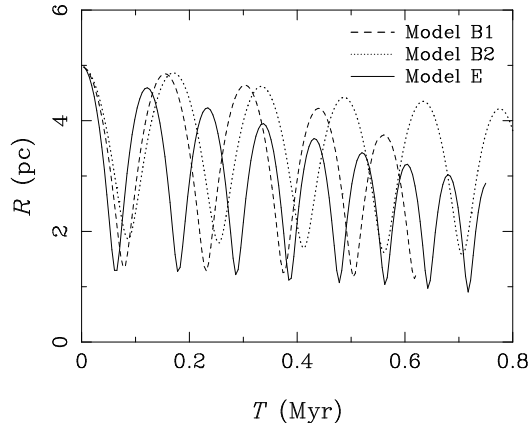


Fig. 11.— The distance of the star cluster from the GC plotted as a function of time. Solid curve shows the result of the galaxy model without the central SMBH (Model E; the same as the solid curve in figure 7). Dashed and dotted curves show the result of the galaxy model with the central SMBH (Model B1 and B2).

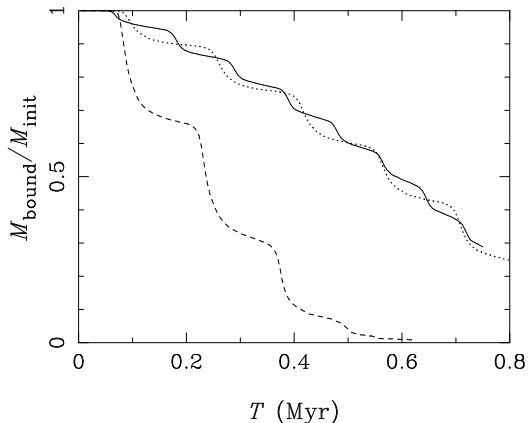


Fig. 12.— The bound mass of the star cluster plotted as a function of time for the galaxy model with the SMBH. Curves have the same meanings as in figure 11.

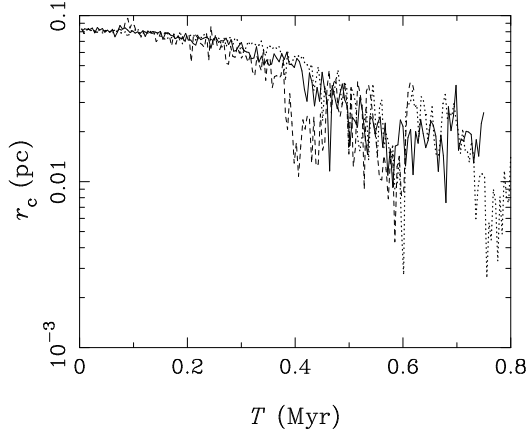


Fig. 13.— The core radius of the star cluster, r_c , plotted as a function of time for the galaxy model with the SMBH. Curves have the same meanings as in figure 11.

The bottom panels show the distribution of all escaped stars at the last snapshots, $T = 0.75$ Myr. Even in the case of the circular orbit (model C), the eccentricities of the escapers in innermost orbits can reach rather large values. However, in the case of the eccentric orbit (model E), the eccentricities of the escapers are even higher. They distribute between 0.4 and 0.8, being consistent with the observed values of stars in the two “disks”. Thus, if the cluster is initially in a highly eccentric orbit, the high eccentricities of observed stars are naturally explained.

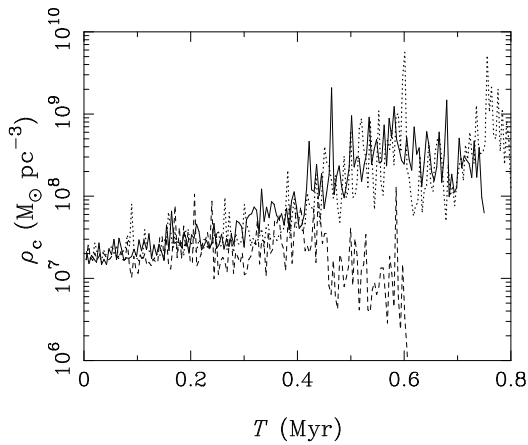


Fig. 14.— The core density of the star cluster, ρ_c , plotted as a function of time for the galaxy model with the SMBH. Curves have the same meanings as in figure 11.

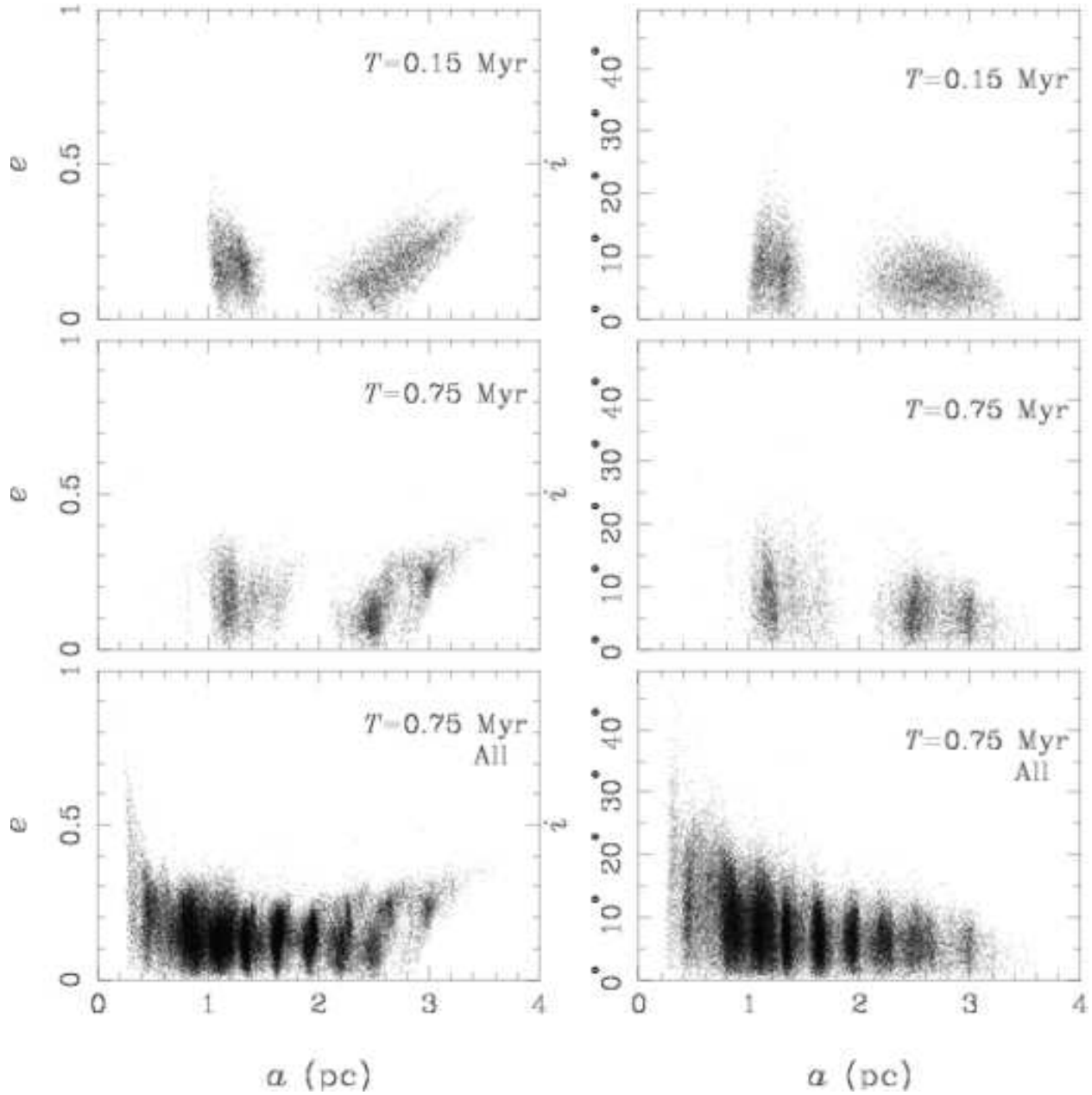


Fig. 15.— The eccentricity (left) and inclination (right) of the stars escaped from the star cluster as the function of their the semi-major axis a for model C (circular orbit). The top panels show the unbound stars at $T = 0.15$ Myr and the middle panels show the position of the same stars shown in top panels, but at $T = 0.75$ Myr. The bottom panels show the all unbound stars at $T = 0.75$ Myr.

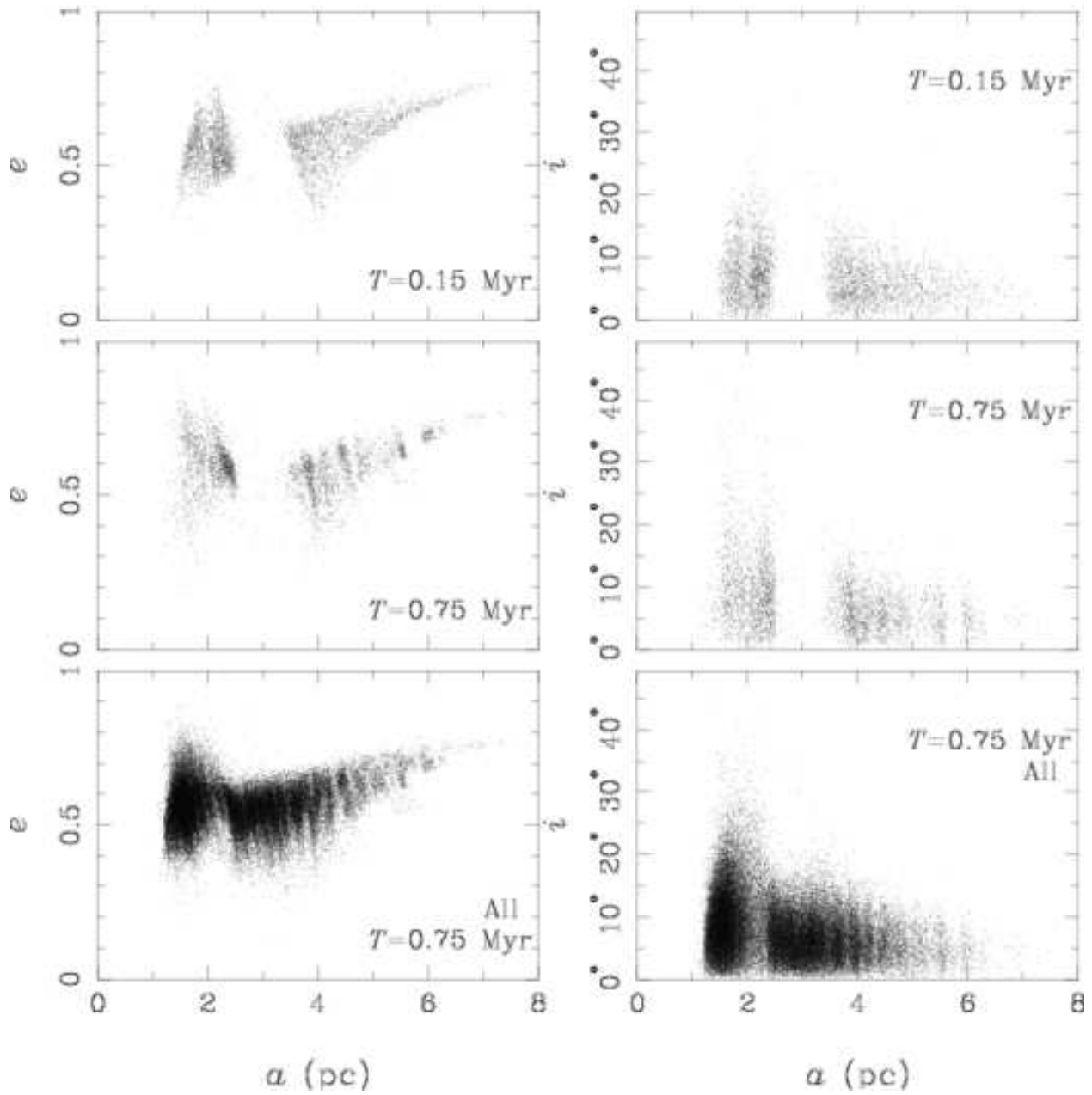


Fig. 16.— Same as figure 15, but for model E (eccentric orbit).

3.4. The Evolution of the Mass Function

Figure 17 shows the evolution of the mass function (MF) of the stars bound to the star cluster for model C. We can see that the slope of the mass function for $m > 10M_\odot$ becomes flatter as the system evolves, while that for $m < 10M_\odot$ shows rather little change. To see this effect more clearly, in figure 18 we plot the fraction of the mass retained in the cluster as the function of the stellar mass for model C. Stars with mass $m > 30M_\odot$ are almost perfectly retained in the cluster, and the retention rate quickly drops in the range of $10M_\odot < m < 30M_\odot$. For $m < 10M_\odot$, retention rate becomes smaller for smaller mass, but the dependence becomes much weaker.

Figure 19 shows the evolution of the enclosed mass in r , the distance from the center of the star cluster for model C. The enclosed masses are calculated for five mass ranges. Initially, all mass ranges have same profile. At $T = 0.15$ Myr, the most massive stars have sank to the center and the second massive stars also shows some central condensation. At $T = 0.45$ Myr, a large fraction of stars more massive than $10 M_\odot$ have sank to the center (within radius 0.02 pc). However, the distribution of stars with mass less than $10M_\odot$ have not changed significantly. Thus, the stars heavier than $10 M_\odot$ remained in the star cluster.

We can estimate the critical mass of the star at which this change in the behavior occurs, by calculating the mass of the star at which the dynamical friction just balances the two-body heating. First, we consider the energy change of the stars in the system consisting of two components with the masses m_1 and m_2 . Assuming that the velocity dispersions of both components are Maxwellian, the mean energy change of a star of mass m_1 is expressed as

$$\left\langle \frac{d}{dt}(m_1 E_1) \right\rangle = \frac{4\sqrt{3\pi}G^2 m_1 m_2 n_2 \log \Lambda}{(\langle E_1 \rangle + \langle E_2 \rangle)^{2/3}} (m_2 \langle E_2 \rangle - m_1 \langle E_1 \rangle), \quad (6)$$

where $\langle E_1 \rangle$ and $\langle E_2 \rangle$ are mean specific kinetic energy of each components, n_2 is the number density of the stars of mass m_2 , and $\ln \Lambda$ is the Coulomb logarithm (Heggie & Hut 2003). At least in the initial model, the velocity dispersion of the stars is independent of the mass. So we can set $\langle E_1 \rangle = \langle E_2 \rangle = 1/2\sigma^2$. In this case, equation (6) is

rewritten as

$$\left\langle \frac{d}{dt}(m_1 E_1) \right\rangle = A n_2 m_1 m_2 (m_2 - m_1), \quad (7)$$

where A is a constant. Now we consider the case of continuous mass distribution, in which the mass distribution of m_2 is given by

$$\frac{dn}{dm} \propto m^{-\alpha}, \quad (8)$$

where C is a constant. The number density of mass m_2 , n_2 , is expressed as

$$n_2 = C m_2^{-\alpha}. \quad (9)$$

By substituting equation (9) to (7) and integrating it over mass m_2 , we can obtain the energy change of stars with mass m_1 as

$$\begin{aligned} \left\langle \frac{d}{dt}(m_1 E_1) \right\rangle &= A' m_1 \int_{m_{\min}}^{m_{\max}} m_2^{-\alpha+1} (m_2 - m_1) dm_2 \\ &\propto m_1 \left[\frac{m_2^{-\alpha+3}}{-\alpha+3} - \frac{m_2^{-\alpha+2}}{-\alpha+2} m_1 \right]_{m_{\min}}^{m_{\max}} \end{aligned} \quad (11)$$

where m_{\max} and m_{\min} are the maximum and minimum mass of the MF and A' is a constant. If the right side of equation (11) is negative, the star with mass m_1 loses energy and sink to the center of the star cluster. The minimum mass with the negative energy change, m_{sink} , is expressed as

$$m_{\text{sink}} = \frac{-\alpha+2}{-\alpha+3} \frac{m_{\max}^{-\alpha+3} - m_{\min}^{-\alpha+3}}{m_{\max}^{-\alpha+2} - m_{\min}^{-\alpha+2}} \quad (12)$$

$$= f(\alpha) m_{\max} \frac{1 - x^{-\alpha+3}}{1 - x^{-\alpha+2}}, \quad (13)$$

where we defined $x \equiv m_{\min}/m_{\max}$ and $f(\alpha) \equiv (-\alpha+2)/(-\alpha+3)$. Using the values used for our model, $m_{\max} = 100M_\odot$, $m_{\min} = 0.3M_\odot$ and $\alpha = 2.35$, we obtain $m_{\text{sink}} = 7.9M_\odot$. This value agrees well with the mass where the power-low index of the MF breaks in figure 18. If $x \ll 1$, we obtain

$$\frac{1 - x^{-\alpha+3}}{1 - x^{-\alpha+2}} = \begin{cases} 1 & (\alpha > 3), \\ -x^{\alpha-2} & (2 < \alpha < 3), \\ x & (\alpha < 2). \end{cases} \quad (14)$$

Therefore,

$$m_{\text{sink}} \simeq \begin{cases} f(\alpha) m_{\min} & (\alpha > 3), \\ -f(\alpha) m_{\min}^{\alpha-2} m_{\max}^{3-\alpha} & (2 < \alpha < 3), \\ f(\alpha) m_{\max} & (\alpha < 2). \end{cases} \quad (15)$$

When $2 < \alpha < 3$, the value of m_{sink} varies from m_{min} to m_{max} .

The observed MF of the stars in the central parsec is much flatter than Salpeter (Paumard et al. 2006). The cluster inspiral model rather naturally explain this flat MF, since only the most massive stars remain bound to the cluster and are carried to the central region of the galaxy.

4. Summary and Discussion

4.1. Summary

We performed fully self-consistent N -body simulations of a star cluster within its parent galaxy and compared the orbital and internal evolutions of the star cluster with those obtained by “traditional” simulations, in which the orbital evolution of the star cluster is calculated from the dynamical friction formula. We confirmed that the inspiral timescale of the star cluster is shorter than that obtained from the “traditional” simulations. Furthermore, our results showed that the core collapse make the core density of the cluster increase and helps the cluster survive.

We performed simulations of circular and eccentric orbits of the star cluster. In previous studies, most of the simulations were from circular orbits (PZ03; Gürkan & Rasio 2005). We found that, however, eccentric orbits are more favorable to explain the distribution of stars around the GC for following reasons.

First, eccentric orbits are natural, if the formation of star clusters was triggered by collisions between gas clouds. Second, star clusters with eccentric orbits can approach to the GC much faster than those with circular orbits (KM03). Third, Paumard et al. (2006) showed that many stars in the counterclockwise rotating disk have high eccentricities ($e \simeq 0.8$), while the distribution of the eccentricities of the stars in the clockwise disk is very broad. Since the eccentricities of the escaped stars distribute around the eccentricity of the star cluster, the star cluster model with eccentric orbits can naturally explain the existence of high-eccentricity stars.

The power-law index of the MF of the bound stars to the star cluster breaks at around $7.9 M_{\odot}$. Stars heavier than this mass sink to the center of the star cluster due to the mass segregation. Since

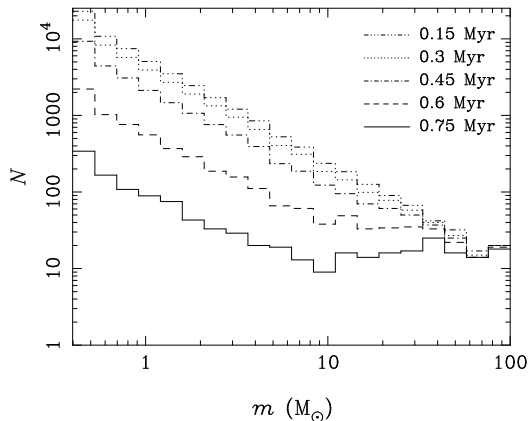


Fig. 17.— The mass function of the bound stars for model C. Times are $T = 0.15, 0.3, 0.45, 0.6,$ and 0.75 Myrs.

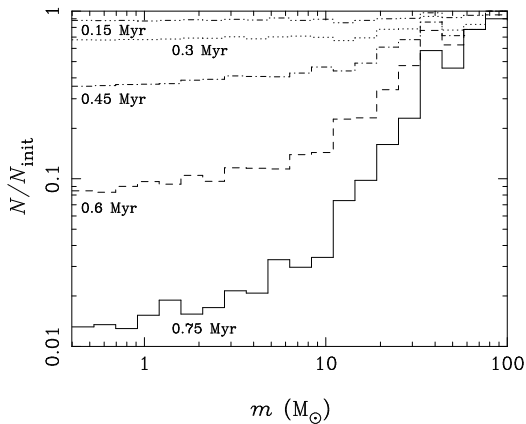


Fig. 18.— The fraction of the mass function of the bound stars to the initial mass function for model C. Times are the same as figure 17.

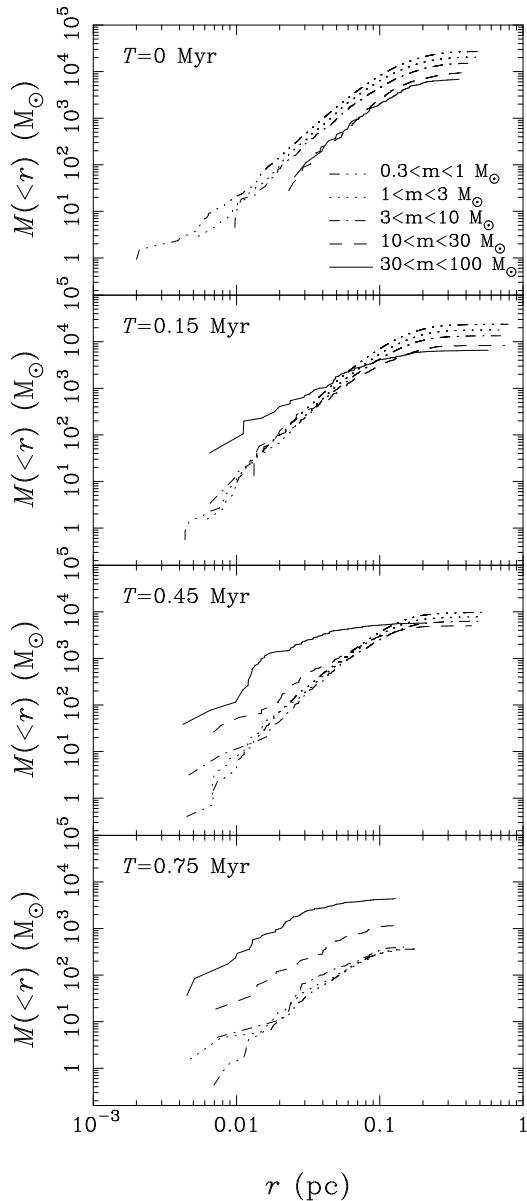


Fig. 19.— The evolution of the enclosed mass of the bound stars for model C.

the tidal stripping removes the stars outside of the star cluster, the massive stars selectively remain in the star cluster. As a result, the star cluster carries only massive stars to the GC. The star cluster scenario can reproduce the flat MF in the central parsec, without the need for nonstandard initial mass function.

4.2. Realistic Model of the Galaxy

First, we showed the orbits of star clusters decays faster in full N -body simulations than in “traditional” simulations, which treat the dynamical friction analytically using a King model $W_0 = 10$ as a model of the central region of the Galaxy. The model is sufficient for such comparisons, but not for more realistic comparison between our model and the stars in the GC because within ~ 1 pc the mass density of our model is much lower than that of the actual Galaxy. Next, we showed the case of more realistic galaxy model with a central BH. The orbital evolution was similar that in the model without a BH. For the comparison between our simulations and the actual stars, however, we need more simulations in various initial conditions. We will report more detail result of runs with the central SMBH in forthcoming papers.

4.3. Formation of an Intermediate-mass Black Hole (IMBH)

IRS 13E consists of seven stars within a projected diameter of ~ 0.02 pc and is located at ~ 0.14 pc in projection from the GC and these stars have very similar proper motions (Maillard et al. 2004; Paumard et al. 2006). Maillard et al. (2004) suggested that IRS 13E is the remnant core of a star cluster that have fallen to the GC and dissolved there and that the members of IRS 13E are bound by a central IMBH. From the analysis of proper motions, the minimum mass of the IMBH was estimated as $1300 M_\odot$ (Maillard et al. 2004) - $10^4 M_\odot$ (Schödel et al. 2005).

In this paper we simulated the evolution of star clusters only before the core collapse because of the limitation of our present code. Our code currently cannot treat the post-collapse evolution since we use the softened potential. Collisions and mergers between stars would have occurred and an IMBH would have be formed, if our code can handle these events. The star cluster inspiral sce-

nario might reveal the origin of the IRS 13E. We are currently working to implement collisions and mergers. The result will be reported in the future papers.

The authors thanks Piet Hut, Keigo Nitadori, and Ataru Tanikawa for useful comments and discussions. M. F. is financially supported by Research Fellowships of the Japan Society for the Promotion of Science (JSPS) for Young Scientists. This research is partially supported by the Special Coordination Fund for Promoting Science and Technology (GRAPE-DR project), Ministry of Education, Culture, Sports, Science and Technology, Japan. Part of calculations were done using the GRAPE system at the Center for Computational Astrophysics (CfCA) of the National Astronomical Observatory of Japan.

REFERENCES

- Barnes, J., & Hut, P. 1986, *Nature*, 324, 446
- Binney, J., & Tremaine S. 1987, *Galactic Dynamics* (Princeton: Princeton Univ. Press), 425
- Chandrasekhar, S. 1943, *ApJ*, 97, 255
- Eisenhauer, F., et al. 2005, *ApJ*, 628, 246
- Figer, D. F. et al. 2002, *ApJ*, 581, 258
- Figer, D. F. 2004, in ASP Conf. Ser. 322, in *The formation and evolution of massive young star clusters*, ed. H. J. G. L. M. Larmers, L. J. Smith, & A. Nota, 49, astro-ph/0403088
- Fujii, M., Funato, Y., & Makino, J. 2006, *PASJ*, 58, 743
- Fujii, M., Iwasawa, M., Funato, Y., & Makino, J. 2007, *PASJ*, 59, 1095
- Fukushige, T., Makino, J., & Kawai, A. 2005, *PASJ*, 57, 1009
- Genzel, R., Pichon, C., Eckart, A., Gerhard, O. E., & Ott, T. 2000, *MNRAS*, 317, 348
- Genzel, R. et al. 2003, *ApJ*, 594, 812
- Gerhard, O. 2001, *ApJ*, 546, L39
- Ghez, A. M., et al. 2003, *ApJ*, 586, L127
- Gürkan, M. A., & Rasio, F. A. 2005, *ApJ*, 628, 236
- Hashimoto, Y., Funato, Y., & Makino, J. 2003, *ApJ*, 582, 196
- Heggie, D. C., & Mathieu, R. D. 1986, in *The Use of Supercomputers in Stellar Dynamics*, ed. P. Hut, and S. McMillan (Lecture Notes in Physics 267; Berlin: Springer), 233
- Heggie, D. C. & Hut, P. 2003, *The gravitational million-body problem* (Cambridge: Cambridge University Press), 159
- Hernquist, L. & Katz, N. 1989, *ApJS*, 70, 419
- Kim, S. S. & Morris, M. 2003, *ApJ*, 597, 312
- Kim, S. S., Figer D. F., & Morris, M. 2004, *ApJ*, 607, L123
- Kinoshita, H., Yoshida, H., & Nakai, H. 1991, *Cel. Mech. and Dyn. Astr.*, 50, 59
- Krabbe, A. et al. 1995, *ApJ*, 447, L95
- Lacy, J. H., Achtermann, J. M., & Serabyn, E. 1991, 380, L71
- Levin, Y. & Beloborodov, M. 2003, *ApJ*, 590, L33
- Lo, K. Y., & Claussen, M. J. 1983, *Nature*, 306, 647
- Lu, J. R., Ghez, A. M., Hornstein, S. D., Morris, M., Thompson, D. J., & Becklin, E. E. 2006, *JPhCS*, 54, 279
- Maillard, J. P., Paumard, T., Stolovy, S. R., & Rigaut, F. 2004, *A&A*, 423, 155
- Makino, J. 1991, *PASJ*, 43, 621
- Makino, J. & Aarseth, S. J. 1992, *PASJ*, 44, 141
- Makino, J., Fukushige, T., Koga, M. & Namura, K. 2003, *PASJ*, 55, 1163
- Makino, J. 2004, *PASJ*, 56, 521
- McMillan, S. L. W. & Aarseth, S. J. 1993, *ApJ*, 414, 200
- McMillan, S. L. W. & Portegies Zwart, S. F. 2003, *ApJ*, 596, 314

- Nagata, T., Woodward, C. E., Shure, M. & Kobayashi, N. 1995, AJ, 109, 1676
- Nayakshin, S. & Sunyaev, R. 2005, MNRAS, 364, L23
- Nayakshin, S., Cuadra, J., & Springel, V. 2007, astro-ph/0701141
- Paumard, T., Maillard, J. P., Morris, M., & Rigaut, F. 2001 A&A, 366, 466
- Paumard, T., Maillard, J. P., & Morris, M. 2004, A&A, 426, 81
- Paumard, T. et al. 2006 ApJ, 643, 1011
- Portegies Zwart, S. F. & McMillan, S. L. W. 2002, ApJ, 576, 899
- Portegies Zwart, S. F., McMillan, S. L. W., & Gerhard, O. 2003, ApJ, 593, 352
- Salpeter, E. E. 1955, ApJ, 121, 161
- Schödel, R., Eckart, A., Iserlohe, C., Genzel, R., & Ott, T. 2005, ApJ, 625, L111
- Spitzer, L. J. & Hart, M. H. 1971, ApJ, 164, 399
- Tuckerman, M. E., Martyna, G. J., & Berne, B. J. 1992, J. Chem. Phys. 97, 1990
- Wisdom, J. & Holman, M. 1991, AJ, 102, 152